Emergence of nonuniform *V*-states by synchronization

L. Friedland
Racah Institute of Physics, Hebrew University of Jerusalem, Jerusalem 91904, Israel

A. G. Shagalov
Institute of Metal Physics, Ekaterinburg 620219, Russian Federation

(Received 20 November 2001; accepted 10 June 2002; published 2 August 2002)

It is shown that a family of nonuniform, *m*-fold symmetric rotating vortex structures in two dimensions (nonuniform *V*-states) can emerge in both free and bounded space by subjecting an axisymmetric vortex with a sharp vorticity edge to external rotation and weak strain of appropriate symmetry. The phenomenon is due to nonlinear synchronization (autoresonance) in the system, as the vorticity distribution of the vortex structure self-adjusts to phase lock with slowly varying external rotation. The synchronization is induced by passage through resonance with the isolated eigenmode of the linearized problem, provided the external strain rate is above a threshold. Synchronized, $m=2$ nonuniform *V*-states remain stable after the external strain is switched off. Free $m=3$ and 4 states, in contrast, are destroyed via three-wave decay at later times. The negative feedback approach is proposed to stabilize this instability. © *2002 American Institute of Physics.* [DOI: 10.1063/1.1497373]

I. INTRODUCTION

Inviscid, vorticity dominated two-dimensional flows often serve as an approximation to physical flows in the atmosphere, oceans, and plasmas. Several types of stable, shape preserving coherent vortex structures are known within this approximation. Classical examples are the monopole, i.e., a single-signed axisymmetric vorticity distribution and the dipole consisting of two adjacent counter-rotating vortices. As the quest for different stable coherent vortex equilibria of two-dimensional Euler equations continued over the years, several other nontrivial examples were found. Shape preserving *V*-states of Deem and Zabusky[1] comprise one such example. The *V*-states are *m*-fold symmetric generalizations of the classical elliptic vortex.[2] The boundary of these *uniform* vortex patches is described by an integrodifferential equation,[3] yielding, for each *m*, a family of rotating solutions depending on a single parameter (say, the rotation frequency of the patch). Numerical studies[1] of *V*-states via contour dynamics (CD) showed that the vortex boundary remained stable with the decrease of its rotation frequency, until it transformed into a curvilinear polygon with included angles of $\pi/2$.[4] No *V*-states existed beyond this stage.

The stability of uniform *V*-states was guaranteed for small perturbations of the vortex boundary. Larger perturbations lead to filamentation instability,[1] so direct realization of the *V*-states is difficult and requires accurate adjustment of nontrivial initial conditions. However, recently proposed nonlinear synchronization (autoresonance) approach[5] has a potential for easing the realization of the *V*-states. The approach is based on starting from a *trivial* (circular) vortex patch and capturing it into resonance with a weak, oscillating external flow of appropriate azimuthal symmetry. The capture is followed by adiabatic deformation of the vortex boundary and emergence of a growing amplitude *V*-state, as the vortex rotation frequency follows the decreasing frequency of the perturbing flow. This automatic phase locking in the driven vortex system comprised an example of a universal nonlinear synchronization phenomenon, leading to coherent pattern formation in different fields of physics. Creation of orbital ellipticity in early dynamics of the solar system,[6] excitation of the diocotron mode in pure electron plasmas,[7] and emergence of quasisolitons in extended systems[8] are other recent examples of this phenomenon.

The present work is devoted to formation and control of *nonuniform V*-states. We shall show that, by starting from an axisymmetric vortex monopole with a sharp vorticity edge and subjecting it to a steady, *m*-fold symmetric *perturbing* flow in combination with a slowly varying external rotation, one can create a family of shape and vorticity distribution preserving nonuniform *V*-states in both free and bounded 2D space regions. Our work is a generalization of the approach used in generating uniform *V*-states.[5] It also relates to recent studies of inviscid 2D vorticity symmetrization. There exist a number of earlier investigations,[9] suggesting that vortices tend to become axisymmetric via cascading filamentation mechanism. On the other hand, stable *uniform V*-states comprise a nonaxisymmetric counter-example. Other such examples are known for a system of superimposed elliptic vortices.[10] A recent study by Dritchel,[11] associates the symmetrization problem to the steepness of vorticity distribution gradients and shows, through CD simulations, that vortices with sufficiently steep edges can remain nonaxisymmetric indefinitely. This conclusion is supported by recent analysis of Schecter *et al.*,[12] who studied relaxation of $m=2$-type vorticity perturbations induced by a fast external impulse. The impulse created a broad spectrum of modes, with exponential decay of asymmetry in the initial relaxation stage. This inviscid damping of asymmetry was attributed to linear mixing of modes, and described in terms of the spectrum of

eigenvalues of linearly perturbed problem.[12] The spectrum had only a continuum of modes for distributions with an extended tail. In contrast, there also was a *discrete* (Kelvin) mode for initial vorticity distributions having a sharp edge. In this case, beyond the initial exponential asymmetry relaxation stage, stable nonaxisymmetric states were observed in simulations and experiments,[12] effect attributed to nonlinear self-trapping phenomenon.

The formation of similar nonaxisymmetric vorticity equilibria is the main goal of the present study. However, instead of using a fast and relatively large impulse, creating a broad spectrum of modes,[12] we shall excite and control a *single*, finite amplitude Kelvin-type mode by applying a *weak* perturbing flow and *passing through resonance* in the system. The method is based on intrinsically nonlinear, persistent synchronization phenomenon, where the excited mode is continuously phase locked with slowly varying external rotation. The external strain, in this excitation process, can be as weak as desired, provided one decreases the sweep rate of the external rotation frequency accordingly. We shall see that the amplitude of the azimuthal deformation of the vortex due to synchronization is mostly defined by how far the external rotation frequency is swept away from the linear resonance. On the other hand, this amplitude will be almost independent of the external strain rate. Therefore, our nonaxisymmetric mode will be near a solution of the unstrained problem at all excitation stages, in contrast to deformations emerging by using other methods. We shall develop our theory for a piecewise constant, initially axisymmetric vorticity distribution representing radially discretized version of a continuous distribution with a sharp edge. Multicontour dynamics simulations are appropriate in this case. Increasing the number of discretization points brings us closer to a continuous distribution, while, in the opposite limit, single- or two-point cases correspond to resonantly driven vortex patch or vortex-inside-vortex problems.

The scope of the paper will be as follows. Section II will present results of our contour dynamics simulations, illustrating a variety of nonuniform *V*-states emerging via nonlinear synchronization. We shall also illustrate a number of phenomena associated with this excitation mechanism, such as the threshold for synchronization and effects of boundary conditions and different time dependences of external rotation frequency. In the process of synchronized evolution described above, we shall excite weakly nonlinear quasinormal modes of the system, having adiabatically varying amplitudes and frequencies. Therefore, in Sec. III, we shall develop a perturbation theory dealing with this adiabatic problem. This step in the theory is equivalent to transition from description via normal modes to WKB (eikonal) approximation in wave physics. To lowest order in this approximation one obtains equations similar to those for normal modes, but having explicitly time dependent parameters. We shall reduce such a lowest order, weakly nonlinear system of equations describing synchronization and control of nonuniform vorticity distributions in Sec. III. In the same section, we shall also test the consistency of our approach by showing that the next order correction in our ''eikonal'' approximation is small. Solutions of the reduced, lowest order phase-amplitude equations describing quasi-Kelvin modes (slowly varying nonuniform *V*-states) in the system and the problem of thresholds for entering nonlinear driven vortex synchronization stage will be discussed in Sec. IV. The issue of stability of the *V*-states with respect to perturbations of different azimuthal symmetry will be dealt with in Sec. V. Finally, Sec. VI presents our conclusions.

II. SYNCHRONIZED NONUNIFORM *V*-STATES VIA CONTOUR DYNAMICS

We proceed from numerical illustrations of our approach to formation of nonuniform *V*-states. Our initial equilibrium is an axisymmetric, monotonically decreasing radial vorticity distribution $\omega(r)>0$ on a compact support $[\omega_{\max}\leqslant\omega(r)<\omega_{\min}$, for $0\leqslant r\leqslant r_{\max}$ and $\omega(r)=0$, for $r>r_{\max}]$. We discretize this distribution and represent it by N centered circular vortices having radii a_n $(0<a_1<a_2<\cdots<a_N=r_{\max})$ and constant vorticities $\omega_1=\frac{1}{2}[\omega_{\max}-\omega(a_2)]$, $\omega_n=\frac{1}{2}[\omega(a_{n-1})-\omega(a_{n+1})]$, $n=2,\cdots,N-1$, and $\omega_N=\frac{1}{2}[\omega(a_{N-1})+\omega(a_N)]$. We subject this vortex pack to external strain and rotation of form

$$\dot{x}=\partial\psi_{\text{ext}}/\partial y+\Omega(t)y,\quad \dot{y}=-\partial\psi_{\text{ext}}/\partial x-\Omega(t)x. \tag{1}$$

Here $(\cdots)=d(\cdots)/dt$ and the stream function, in polar coordinates, is

$$\psi_{\text{ext}}=\epsilon R^2(r/R)^m\cos(m\varphi). \tag{2}$$

The external rotation was in the direction opposite to that of the free vortex (i.e., $\Omega>0$) and its frequency depended on time, while ϵ was constant, but small enough to view the strain contribution to vortex dynamics as a perturbation. Such perturbing flows can be realized in experiments. Indeed, any azimuthally asymmetric, stream function prescribed on a cylindrical boundary of radius $R>r_{\max}$ generates, inside the cylinder, a linear superposition of stream functions of type (2) with different m. Only $nm'(n=1,2,\ldots)$ components will be present in this superposition if the boundary conditions will have m'-fold azimuthal symmetry. We shall study resonant effects associated with $n=1$ component of such a perturbing flow. Then, the effect of $n>1$ terms on our vortex dynamics can be neglected since these terms are nonresonant and small compared to $n=1$, if $r_{\max}/R\ll 1$.

Figures 1(b)–1(d) show $m=2$, 3, and 4 multicontour states excited in our CD simulations. All these states emerged by starting from the *same* five uniform vortex patches having contours shown in Fig. 1, representing a discretized version of the vorticity distribution of form[11]

$$\omega(r)=\begin{cases}\omega_0[1-\kappa(r/r_{\max})^2], & 0\leqslant r\leqslant r_{\max},\\ 0, & r>r_{\max},\end{cases} \tag{3}$$

where parameter $\kappa=0.6$ and radii $a_n=0.2nr_{\max}$, $n=1,\ldots,5$. The external rotation frequency varied linearly in time, $\Omega(t)=\Omega_0-\alpha t$, and, for each m, slowly passed through frequency Ω_0 of the corresponding linear *discrete* mode of the undriven system (see the next section explaining our choice of Ω_0). We used dimensionless time t ($\omega_0 t$ in previous notations) in our calculations and

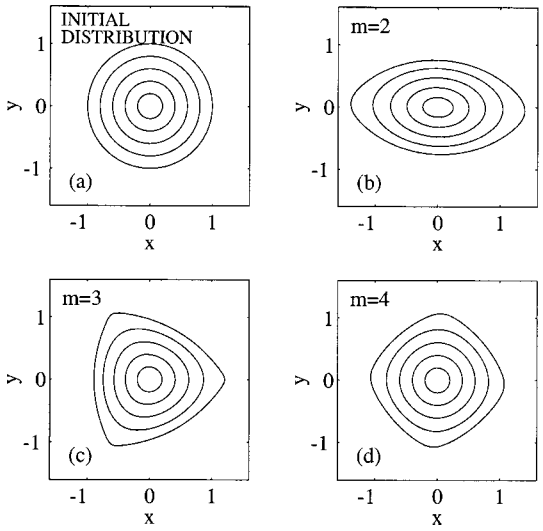

FIG. 1. Nonuniform V-states of different symmetry. (a) Initial axisymmetric vorticity distribution; (b) $m=2$; (c) $m=3$; (d) $m=4$. These V-states emerged by passage through resonance and synchronization by starting from the same vorticity distribution shown in (a).

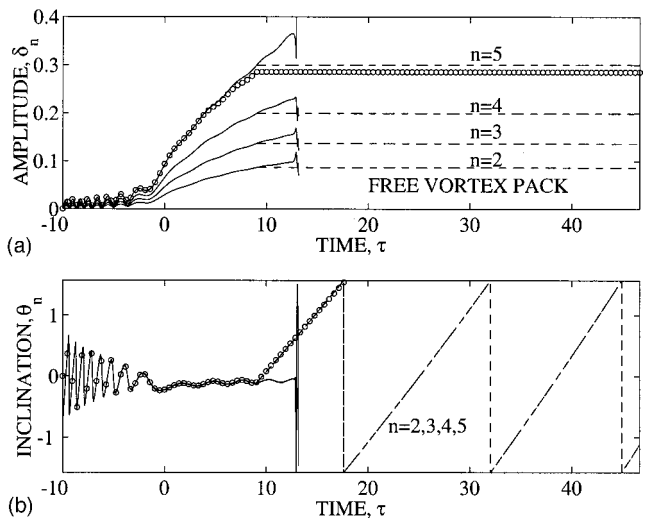

FIG. 2. The excitation of $m=2$ multicontour V-state by passage through resonance. (a) Deformation amplitudes of the four outer contours, $n=2,3,4,5$; (b) inclinations of the contours. All inclinations are nearly the same, individual vortices are mutually phase locked. The solid lines: continuing linear sweep of external rotation frequency. The multicontour state in this case is phase locked with the rotation, until filamentation instability at $\tau=12.5$. The dashed lines represent the straining flow and variation of external rotation frequency are switched off beyond $\tau=9$. Uniformly rotating, free nonuniform V-state is stable in this case. (○) calculations using reduced theory.

viewed x, y, r, a_n, ϵ, α, Ω, Ω_0 (and ω_n in the following) as dimensionless and representing $x/r_{\max}$, $y/r_{\max}$, $r/r_{\max}$, $a_n/r_{\max}$, ϵ/ω_0, α/ω_0^2, Ω/ω_0, Ω_0/ω_0 (and ω_n/ω_0) previously. The dimensionless Ω, Ω_0, and ω_n were all of $O(1)$, while ϵ, $\alpha \ll 1$. Therefore, the external strain acted as a perturbation and the external rotation frequency varied adiabatically. This adiabaticity yielded another slow time scale $\alpha^{-1/2}$ in the problem, so we presented our results as functions of slow time $\tau=(m\alpha)^{1/2}t$. The starting time in all our simulations was $\tau=\tau_0=-10$. We used dimensionless adiabaticity and strain rate parameters $m\alpha=\frac{1}{9}\times 10^{-4}$ and $\mu=m\epsilon(r_{\max}/R)^{m-2}=3\times 10^{-4}$ for all m. Note that $\alpha/\mu \ll 1$ in our calculations, so the strain parameter was always the largest of the two small parameters in the problem. The dimensionless resonant frequencies (see Sec. IV) were $\Omega_0=0.201$, 0.258, and 0.284 for $m=2$, 3, and 4, respectively. Finally, we switched off the external strain and held the rotation frequency constant at $\tau>\tau_1$ beyond the resonance (τ_1 was 9.0, 5.0, and 1.6 for $m=2$, 3, and 4, respectively). The form of the boundaries of individual vortices in the vortex packs for different m at these values of τ_1 are shown in Figs. 1(b)–1(d).

Additional details from our simulations in the $m=2$ case are shown in Figs. 2(a) and 2(b). Figure 2(a) shows the time evolution of the deformation amplitudes [defined as $\delta_n=\frac{1}{2}(r_{n\,\max}-r_{n\,\min})$] of the boundaries of the outer four vortices comprising the vortex pack ($n=2,3,4,5$), while Fig. 2(b), shows the inclination angles θ_n of individual contours in the multicontour state, defined as the angular coordinates of the maximum radius $r_{\max}$ of each patch in the sector $|\varphi|<\pi/m$ in the rest frame. One can see excitation of a nonuniform multicontour structure, with monotonically increasing δ_n beyond the linear resonance. One can also see in Fig. 2(b) that all inclinations are nearly the same, so the vortices in the pack are mutually phase locked at all times. In addition, the whole pack is phased locked near $\theta \approx 0$, for $\tau_1>\tau>0$ with the external rotation, as it self-adjusts its angular velocity to synchronize (stay in resonance) despite variation of the rotation frequency. As described above, the external strain and the variation of the external rotation were turned off in the figure at $\tau_1=9$. Beyond this time (see dashed lines in Fig. 2), the resulting state preserved its form [shown in Fig. 1(b)], i.e., all δ_n remained constant and the pack rotated uniformly [see Fig. 2(b)] for at least 300 rotation periods of a free vortex state. Deviations were observed at some later time, but this time could be always increased by increasing the accuracy of the simulations. Thus, we attributed these deviations to numerical instabilities. We used a standard CD algorithm[13,14] and tested the accuracy by both increasing the number of points on the contour and decreasing the integration time step. If the straining flow was left present beyond τ_1, and the decrease of the external rotation frequency continued (we show this case in Fig. 2 by full lines ending at $\tau \approx 12.5$), the outer vortex was driven into curvilinear polygon stage with including angles of $\pi/2$. Soon after we observed development of filaments, dispersing the corners of the vortex, destructing synchronization, and destroying the coherent state. The circles in Fig. 2 represent the results of calculations obtained by using our reduced theory [solutions of Eqs. (35) and (36) in Sec. IV] and we see a good agreement with the simulation results.

We have performed simulations similar to those shown in Fig. 2 for $m=3$, 4, and 5 finding both similarities and remarkable differences as compared to the $m=2$ case. First of all, the maximum excitation amplitude of the coherent (phase-locked) state prior to filamentation was different for different m and initial vorticity distributions. Figure 3 shows these maximum values $\delta_{\max}$ obtained numerically for the

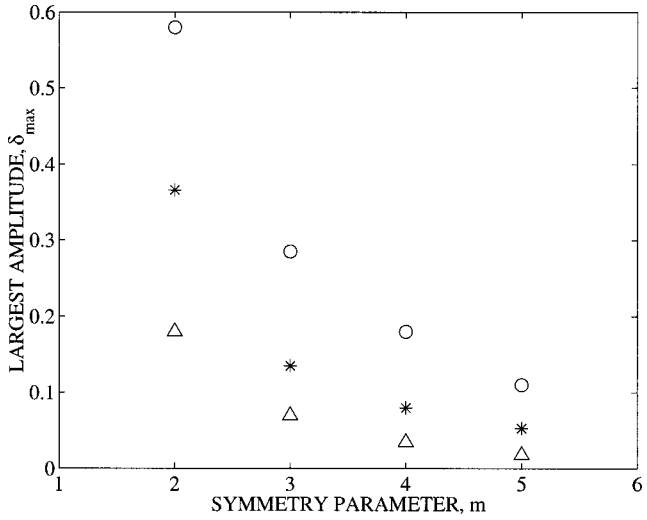

FIG. 3. The largest excitation amplitudes of the outer ($n=5$) vorticity contour of nonuniform *V*-states emerging by passage through resonance by linear sweep of the external rotation frequency and different initial vorticity distributions. (○) $\kappa=0$ (this case corresponds to a single uniform patch); (*) $\kappa=0.6$; (△) $\kappa=1.0$.

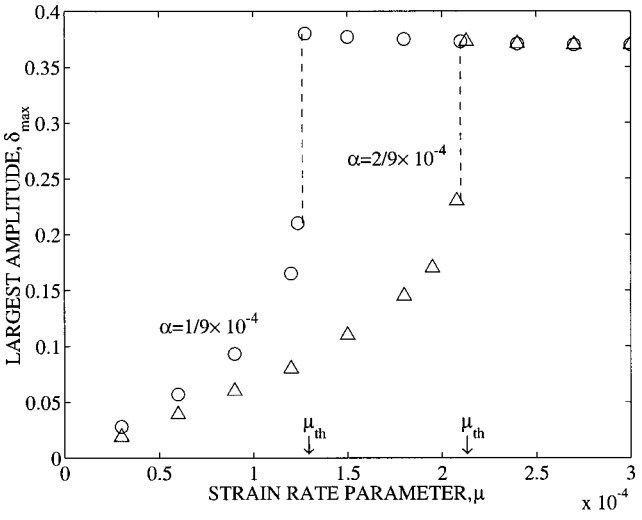

FIG. 5. The threshold phenomenon. The dependence of the largest deformation amplitude δ_{max} of the outer ($n=5$) contour on the strain rate parameter in $m=2$, $\kappa=0.6$ case for two different external rotation sweep rates $\alpha=(1/9,2/9)\times10^{-4}$. Below the threshold, the phase locking with the external rotation discontinues at $\tau>0$ and deformation amplitude saturates much below the filamentation level.

outer vortex ($n=5$) in the pack. Our second observation was the instability of free nonuniform $m>2$ *V*-states emerging by synchronization. We illustrate this effect in Fig. 4, showing results of our simulations for $m=3$ case for deformation amplitudes of the $n=5$ and 3 vortices in the pack. The remaining patches in the pack evolved similarly. The curves (a) in the figure represent the case of continuing presence of the external strain and continuing linear sweep of the external rotation. The *V*-state in this case is destroyed by filamentation instability at $\tau\approx7$. In contrast to (a), curves (b) and (c) in the figure represent cases, when the external strain and external rotation sweep were turned off at $\tau=3.3$ and 0.5, respectively. We see evolution of free *V*-states of two different amplitudes and, in contrast to $m=2$ case, observe instability destroying these nonuniform states at longer times (still the free *V*-states are well preserved for at least 60 rotations of the free vortex). We shall discuss this instability and suggest a method of stabilization in Sec. V, allowing creation and long time control of *V*-states for $m>2$ via synchronization approach.

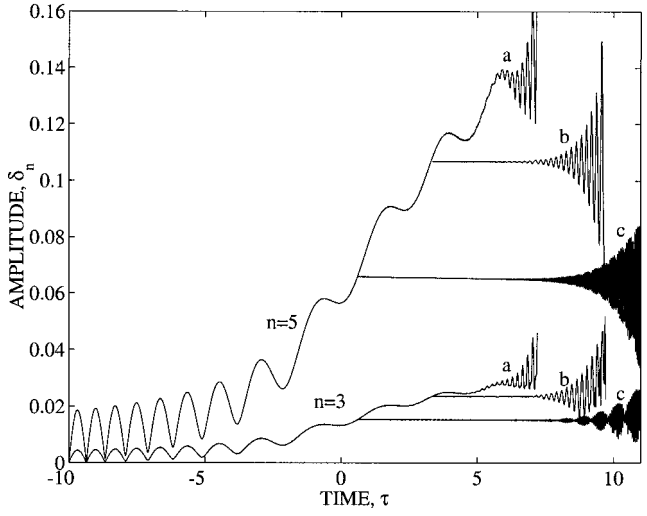

FIG. 4. The evolution of deformation amplitudes of $n=5$ and $n=3$ contours of $m=3$ *V*-state. Remaining contours evolve similarly. Curves (a) Continuing linear sweep of the external rotation frequency; (b) the straining flow and variation of external rotation frequency are switched off beyond $\tau=3.3$; (c) the strain and variation of external rotation are switched off beyond $\tau=0.5$. Free $m=3$ nonuniform states are unstable, in contrast to $m=2$ case. The instability destroys larger amplitude *V*-states first.

Additional important feature characteristic of adiabatic synchronization discussed above was the existence of a threshold μ_{th} on the strain rate parameter for continuing phase locking by passage through resonance. This phenomenon is illustrated in Fig. 5, showing the dependence of the largest deformation amplitude of the outer contour in the *V*-state on the strain rate parameter μ in $m=2$ case for two different external rotation sweep rates $\alpha=(1/9,2/9)\times10^{-4}$. We used vorticity distribution with $\kappa=0.6$ in these calculations. We found that the threshold was very sharp and below the threshold the phase locking with the external rotation discontinued for $\tau>0$, while the amplitude saturated at values below the filamentation level. We shall discuss this threshold phenomenon in more detail in Sec. IV.

The *linear* sweep $\Omega(\tau)=\Omega_{m0}-(\alpha/m)^{1/2}\tau$ of the external rotation frequency in all our examples above was a choice, easing theoretical modelling in the following. Nonetheless, this linear dependence of $\Omega(\tau)$ was not a necessity for emergence and control of resonantly trapped nonuniform *V*-states. After the trapping, one could vary the external frequency as desired without losing the phase locking, as long as the variation of $\Omega(\tau)$ was sufficiently slow. In contrast to other methods of excitation of nonaxisymmetric vortex deformations (e.g., Ref. 12), we could also return to nearly original axisymmetric state by simply reversing the direction of variation of Ω. This is illustrated in Fig. 6, showing the evolution of the five vortex pack in the $m=2$ case, for the

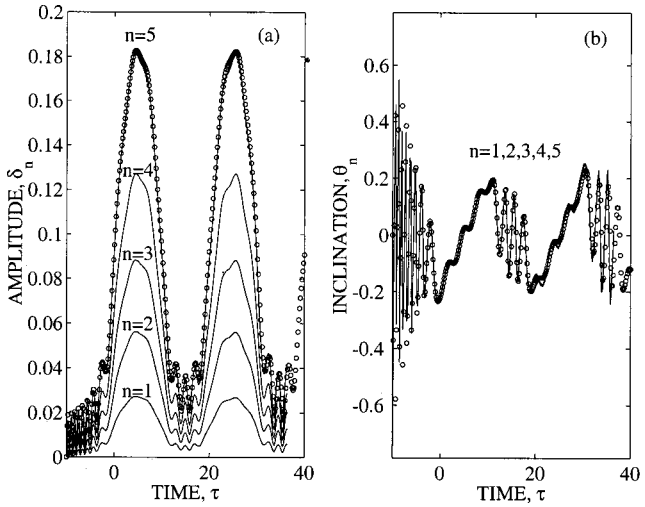

FIG. 6. Two successive excitation and de-excitation stages (solid lines) of $m=2$ V-state ($\kappa=0.6$ case) for oscillating external rotation frequency. (a) Amplitudes; (b) inclinations. The vortices are phase-locked both mutually and with the external rotation. (○) Calculations using reduced theory.

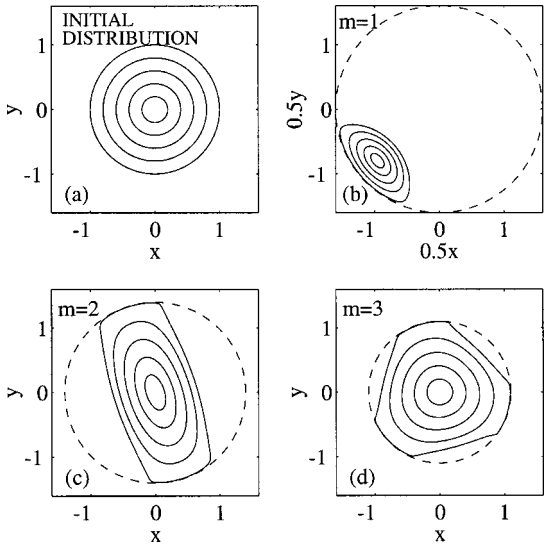

FIG. 7. Nonuniform V-states in bounded space (the associated stream functions vanish on circular boundaries shown by dashed lines). (a) Initial axisymmetric vorticity distribution; (b) $m=1$ diocotron mode, this mode rotates due to interaction between the vortex and its image charge (the axis in this case are rescaled for better exposition); (c) $m=2$; (d) $m=3$. All these V-states emerge by passage through resonance and synchronization, starting from the same vorticity distribution shown in (a).

same initial conditions and parameters as in Fig. 2, using the linear dependence of $\Omega(\tau)=\Omega_{m0}-(\alpha/m)^{1/2}\tau$ for $\tau<0$, but oscillating the external rotation frequency as $\Omega(\tau)=\Omega_{m0}-(\alpha/m)^{1/2}(T/2\pi)\sin(2\pi\tau/T)$, $T=20$ for $\tau>0$. Two stages of stable excitations and de-excitations of the V-state can be seen in Fig. 6 during successive oscillation periods of $\Omega(\tau)$. We note that at all evolution stages, the patches in the vortex pack are mutually phase locked (have nearly the same inclinations) and the whole pack is continuously phase-locked with the external rotation despite the variation of the parameters of the system. The circles in this figure represent the results obtained by using our reduced theory (see Sec. IV), again showing excellent agreement with simulations.

The last illustration in this section, Fig. 7, tests our assumption of the absence of boundaries in exciting nonuniform V-states. The boundaries are important in many nonneutral plasma applications, where, typically, one confines the plasma inside a grounded cylindrical wall, defining the electric potential (the analog of the stream function in fluid applications) inside the cylinder. Figure 7 shows examples of $m=1$, 2, and 3 states in a bounded region with the stream functions vanishing on a circle (the dashed lines in the figure). We applied again the synchronization approach in generating all these examples, started from the same initial vorticity distribution as in Fig. 1, used external strains having appropriate azimuthal symmetries, and swept the external rotation frequency linearly. The parameters in these calculations were $\mu=2.5\times10^{-3}$, 3.6×10^{-4}, 3.6×10^{-4}, $\alpha=\frac{1}{5}\times10^{-4}$, $\frac{1}{18}\times10^{-4}$, $\frac{1}{27}\times10^{-4}$, and dimensionless radius of the boundary $R_b=3.2$, 1.4, 1.1 for $m=1,2,3$, respectively. The $m=1$ case in the figure is particularly interesting. It exists in its rotating form in the bounded case only. The reason for the rotation of this vortex along the boundary is interaction with its image charge. In pure electron plasmas this state corresponds to $m=1$ diocotron mode, which has been studied recently in the context of the nonlinear synchronization approach.[7] For other m, uniformly rotating V-states shown in Fig. 7 remained synchronized, until driven into stage destructed by filamentation (the structures shown in the figure are those just prior to this stage). All these examples lead to an important conclusion that synchronization approach to excitation of nonaxisymmetric vortices works also in the presence of a boundary. We shall not discuss bounded V-states in more detail in this work, leaving the results shown in the figure as illustrations of possible uses of resonant capture and adiabatic control method. The following presentation will focus on vortices in free space only. The next section introduces our reduced theory of excitation of such nonuniform V-states by synchronization.

III. REDUCED MULTICONTOUR SYSTEM

This section presents our formal approach to studying excitation of synchronized, nonuniform V-states. We proceed from the simplest problem of a V-state composed of two centered vortex patches, initially having circular forms (radii $a_1<a_2$) and constant vorticities $\omega_{1,2}$. The boundaries of the vortices are written in polar coordinates[3]

$$r_n=p_n+\delta_n\cos(m\varphi_n)+h_n\delta_n^2\cos(2m\varphi_n)+O(\delta_n^3), \quad (4)$$

where $n=1,2$, $\varphi_n=\varphi-\theta_n$, θ_n are inclination angles of the nth vortex, and δ_n represent *small* expansion amplitudes. We assume m-fold symmetric form of the boundary (4), in agreement with the symmetry of the external strain (2). The amplitudes δ_n, and the inclination angles θ_n are functions of time. Since the area of each vortex patch is conserved despite the external strain and rotation, we have

$$p_n^2=a_n^2-\tfrac{1}{2}\delta_n^2+O(\delta_n^4). \quad (5)$$

Later, we will need the angular momentum of our system of vortices. The angular momentum of each patch is P_n

$=(\omega_n/2)\int r^2\,dS$, where the integration is over the area of the patch. Thus, $P_n=(\omega_n/8)\int_0^{2\pi} r_n^4\,d\varphi$, which upon substitution of (4) and (5), yields

$$P_n=\frac{\pi\omega_n}{4}(a_n^4+2a_n^2\delta_n^2)+O(\delta_n^4). \tag{6}$$

We seek dynamical description of our driven system to $O(\delta_n^3)$. However, even to this order, self-consistent inclusion of nonlinear terms is algebraically complex (see, for example, the developments for a single driven vortex patch[5]). Therefore, we proceed from a simpler *linear* excitation problem and include the nonlinearity later by using heuristic arguments. The linearly perturbed stream functions associated with each of the two vortices are[15]

$$\psi_n=\begin{cases}\dfrac{\omega_n}{4}(a_n^2-r^2)+\dfrac{\omega_n a_n\delta_n}{2m}\left(\dfrac{r}{a_n}\right)^m\cos m\varphi_n, & r<a_n,\\ -\dfrac{\omega_n a_n^2}{2}\ln\left(\dfrac{r}{a_n}\right)+\dfrac{\omega_n a_n\delta_n}{2m}\left(\dfrac{a_n}{\tau}\right)^m\cos m\varphi_n, & r>a_n.\end{cases} \tag{7}$$

Our goal is to describe self-consistent dynamics of $\delta_n(t)$ and $\theta_n(t)$ as given by the external rotation and flow associated with the full stream function $\Psi(r,\varphi)=\psi_1(r,\varphi)+\psi_2(r,\varphi)+\psi_{\text{ext}}(r,\varphi)$ in the problem. The evolution equations for δ_n and θ_n can be obtained by imposing preservation of the functional form (4) of the two perturbed boundaries at all times in the presence of the external strain and rotation. For example, for the vortex boundary, we require (to lowest order $p_1=a_1$):

$$F_1(t,r_1,\varphi)\equiv a_1+\delta_1(t)\cos(m\varphi_1)-r_1\equiv 0 \tag{8}$$

at all times, where $\varphi_1=\varphi-\theta_1(t)$, or

$$\partial F_1/\partial t+\dot r_1\partial F_1/\partial r_1+\dot\varphi\partial F_1/\partial\varphi=0. \tag{9}$$

Here the flow

$$\dot r_1=\frac{1}{r_1}\frac{\partial\Psi_1}{\partial\varphi}$$

and

$$\dot\varphi=-\Omega-\frac{1}{r_1}\frac{\partial\Psi_1}{\partial r_1}$$

on the first vortex boundary is generated by the external rotation and the full stream function $\Psi_1=\Psi(r_1,\varphi)$. Then, to $O(\delta_n)$, one obtains

$$\dot\delta_1=-\frac{\omega_2}{2}\delta_2\left(\frac{a_1}{a_2}\right)^{m-1}\sin m\Delta\theta-\mu a_1^{m-1}\sin m\theta_1, \tag{10}$$

$$\delta_1\dot\theta_1=\left(\Omega_1-\Omega+\frac{\omega_2}{2}\right)\delta_1-\frac{\omega_2}{2m}\delta_2\left(\frac{a_1}{a_2}\right)^{m-1}\cos m\Delta\theta-(\mu/m)a_1^{m-1}\cos m\theta_1, \tag{11}$$

where $\Delta\theta=\theta_1-\theta_2$, and $\Omega_1=\omega_1(m-1)/2m$ is the rotation frequency of m-fold symmetric perturbation of a single vortex.[15] By defining $Z_n=\delta_n\exp(im\theta_n)$, $n=1,2$, we can rewrite Eqs. (10) and (11) in a more compact form

$$\dot Z_1=i[(M_{11}-m\Omega)Z_1+M_{12}Z_2-B_1], \tag{12}$$

where $M_{11}=m(\Omega_1+\omega_2/2)$, $M_{12}=-(\omega_2/2)(a_1/a_2)^{m-1}$, and $B_1=\mu a_1^{m-1}$. Similar developments for the second vortex yield

$$\dot Z_2=i[M_{21}Z_1+(M_{22}-m\Omega)Z_2-B_2], \tag{13}$$

where $M_{22}=m[\Omega_2+(\omega_1/2)(a_1/a_2)^2]$, $M_{21}=-(\omega_1/2)\times(a_1/a_2)^{m+1}$, $\Omega_2=\omega_2(m-1)/2m$, and $B_2=\mu a_2^{m-1}$.

Next, we write Eqs. (12) and (13) in matrix notations

$$\dot{\mathbf{Y}}=i[\mathbf{M}\cdot\mathbf{Y}-\dot{\mathbf{B}}e^{im\int\Omega(t)dt}], \tag{14}$$

where $\mathbf{Y}=\mathbf{Z}\exp[im\int\Omega(t)dt]$ and generalize the problem to N vortices. In this case Eq. (14) holds for $Y_n=\delta_n\exp\{i[\theta_n+im\int\Omega(t)dt]\}$, $B_n=\mu a_n^{m-1}$, $n=1,\cdots,N$, while

$$M_{kn}=\begin{cases}-(\omega_n/2)(a_k/a_n)^{m-1}, & n>k,\\ -(\omega_n/2)(a_n/a_k)^{m+1}, & n<k,\end{cases}$$

and

$$M_{kk}=\frac{1}{2}m\left[\omega_k(1-1/m)+\sum_{j=1}^{k-1}\omega_j(a_j/a_k)^2+\sum_{j=k+1}^{N}\omega_j\right].$$

Finally, we include nonlinearity, by adding a small, $O(\delta^3)$ term $\mathbf{H}$ in (14):

$$\dot{\mathbf{Y}}=i[\mathbf{M}\cdot\mathbf{Y}-\mathbf{B}e^{im\int\Omega(t)dt}+\mathbf{H}]. \tag{15}$$

In components, $H_l=G_{ljnk}Y_jY_n^*Y_k$, $l=1,\ldots,N$, where G_{ljnk} are constant coefficients, the summation convention is used for repeated indices in the definition of H_l, and we assume $G_{ljnk}=G_{jlkn}^*$. This symmetry is chosen to represent conservative resonant interactions of our system of vortices, with all patches having nearly equal inclination angles θ_n (see below).

Our next step is symmetrization of our equations by rescaling of $\mathbf{Y}$. We define $\mathbf{W}=\mathbf{Q}\cdot\mathbf{Y}$, where matrix $\mathbf{Q}$ is diagonal and $Q_{nn}=\omega_n a_n^2$, $n=1,\cdots,N$. Then (15) yields

$$\mathbf{Q}^{-1}\cdot\dot{\mathbf{W}}=i[\mathbf{M}'\cdot\mathbf{W}+\mathbf{H}'-\mathbf{B}e^{im\int\Omega(t)dt}], \tag{16}$$

where $H_l'=G_{ljnk}'W_jW_n^*W_k$, the coefficients $G_{ljnk}'=(Q_{jj}Q_{nn}Q_{kk})^{-1}G_{ljnk}$, and the matrix $\mathbf{M}'=\mathbf{M}\cdot\mathbf{Q}^{-1}$ is *symmetric* and real

$$M_{kn}'=M_{nk}'=-\tfrac{1}{2}(a_na_k)^{-1}(a_n/a_k)^m,\quad k>n. \tag{17}$$

Due to the symmetries of $\mathbf{M}'$ and $G_{ljnk}(G_{ljnk}=G_{jlkn}^*)$, Eq. (16) yields the conservation law in the absence of the external strain ($\mathbf{B}=\mathbf{0}$):

$$\mathbf{J}=\mathbf{W}^\dagger\cdot\mathbf{Q}^{-1}\cdot\mathbf{W}=\sum\omega_n a_n^2\delta_n^2=\text{const}. \tag{18}$$

This result represents conservation of the total angular momentum $P=\frac{1}{2}\Sigma\int\omega_n r^2\,dS_n$ in the system. In fact, the total momentum of our system of interacting vortices in the $\mathbf{B}=\mathbf{0}$ case must be conserved to all orders in δ.[16] But [see (6)]

$$P=\frac{\pi}{4}\left(\sum\omega_n a_n^4+2\sum\omega_n a_n^2\delta_n^2\right)+O(\delta_n^4), \tag{19}$$

and, therefore, $(\pi/2)\mathbf{J}$ represents the *excess* of the momentum [correct to $O(\delta^3)$] in the vortex pack due to the perturbations of the circular boundaries of its components. Consequently, Eq. (18), obtained by using the assumed symmetry of coef-

ficients G_{jnlk} in $O(\delta^3)$ term $\mathbf{H}$ in (15), justifies our choice of this symmetry. Note also that, because of the positiveness of ω_i, Eq. (18) guarantees quasilinear stability of the perturbed, single m vorticity distribution.

Next, we proceed to the analysis of solutions of Eq. (16). We seek a solution of form $\mathbf{W}=\mathbf{A}\exp(i\Theta)$, where $\mathbf{A}$ is assumed to be a *slow* function of time, while $\dot{\Theta}=\Lambda$ is one of the N eigenvalues of matrix $\mathbf{M}$ (since $\mathbf{M}$ has dimensionality of frequency, the term *eigenfrequency* will be used for Λ in the following). Then Eq. (16) yields

$$-\mathbf{Q}^{-1}\cdot\dot{\mathbf{A}}+i\mathbf{D}\cdot\mathbf{A}+i\tilde{\mathbf{H}}=i\mathbf{B}e^{i[m\int\Omega(t)dt-\Theta]}, \tag{20}$$

where $\tilde{H}_l=G'_{ljnk}A_jA_n^*A_k$ and

$$\mathbf{D}=\mathbf{M}'-\Lambda\mathbf{Q}^{-1}. \tag{21}$$

By definition,

$$\det\mathbf{D}=\det\mathbf{Q}^{-1}\det(\mathbf{M}-\Lambda\mathbf{I})=0. \tag{22}$$

Furthermore, because of the symmetry of $\mathbf{M}'$, all eigenfrequencies Λ are real.

Now, we introduce dimensionless parameter $\sigma\ll 1$ describing the slowness of evolution of $\mathbf{A}$ and view both the driving and the nonlinear terms in the right-hand side of Eq. (20) as, formally, of $O(\sigma)$. This scaling allows to solve Eq. (20) perturbatively. We expand

$$\mathbf{A}=\mathbf{A}_0+\mathbf{A}_1+\mathbf{A}_2+\cdots, \tag{23}$$

where the terms are ordered in powers of σ. Then, to zero order,

$$\mathbf{D}\cdot\mathbf{A}_0=0, \tag{24}$$

yielding, because of (22), a nontrivial solution $\mathbf{A}_0$. To first order,

$$i\mathbf{D}\cdot\mathbf{A}_1=\mathbf{Q}^{-1}\cdot\dot{\mathbf{A}}_0-i\tilde{\mathbf{H}}^0+i\mathbf{B}e^{i[m\int\Omega(t)dt-\Theta]}, \tag{25}$$

where $\tilde{H}_l^0=G'_{ljnk}A_{0j}A_{0n}^*A_{0k}$. Next, we express our symmetric $N\times N$ real matrix $\mathbf{D}$ in terms of its eigenvalues ϵ_n (all real) and eigenvectors $\mathbf{e}_n$ (real and orthonormal $\mathbf{e}_i^T\cdot\mathbf{e}_j=\delta_{ij}$):

$$\mathbf{D}=\epsilon_1\mathbf{e}_1\mathbf{e}_1^T+\epsilon_2\mathbf{e}_2\mathbf{e}_2^T+\cdots. \tag{26}$$

We also express the zero order solution as

$$\mathbf{A}_0=\alpha_1\mathbf{e}_1+\alpha_2\mathbf{e}_2+\cdots. \tag{27}$$

Since

$$\det\mathbf{D}=\epsilon_1\epsilon_2\epsilon_3\cdots=0, \tag{28}$$

at least one of the eigenvalues, say ϵ_1, vanishes and we shall assume that the rest of the eigenvalues are finite for simplicity. Then, on substituting (27) into (24), we have $\epsilon_1\alpha_1\mathbf{e}_1+\epsilon_2\alpha_2\mathbf{e}_2+\cdots=0$, and, therefore, $\alpha_1\neq 0$, $\alpha_2=\alpha_3=\cdots=0$. Consequently,

$$\mathbf{A}_0=\alpha_1\mathbf{e}_1. \tag{29}$$

Similarly, in first order, we write

$$\mathbf{A}_1=\gamma_1\mathbf{e}_1+\gamma_2\mathbf{e}_2+\cdots,$$

$$\mathbf{B}=\beta_1\mathbf{e}_1+\beta_2\mathbf{e}_2+\cdots.$$

Then, by multiplying (25) by $\mathbf{e}_i^T$ from the left, we obtain

$$0=\mathbf{e}_1^T\cdot\mathbf{Q}^{-1}\cdot\mathbf{e}_1\dot{\alpha}_1+i\beta_1e^{i[m\int\Omega(t)dt-\Theta]}-ig_1|\alpha_1|^2\alpha_1$$

and

$$i\epsilon_i\gamma_i=\mathbf{e}_i^T\cdot\mathbf{Q}^{-1}\cdot\mathbf{e}_1\dot{\alpha}_1+i\beta_ie^{i[m\int\Omega(t)dt-\Theta]}-ig_i|\alpha_1|^2\alpha_1$$

for $i>1$, where $g_i=G_{ljnk}e_{il}e_{1j}e_{1n}e_{1k}$. The first equation in this system describes slow evolution of the zero order amplitude α_1:

$$\dot{\alpha}_1=-ip|\alpha_1|^2\alpha_1+i\eta e^{i[m\int\Omega(t)dt-\Theta]}, \tag{30}$$

where $p=-g_1(\mathbf{e}_1^T\cdot\mathbf{Q}^{-1}\cdot\mathbf{e}_1)^{-1}=g_1(\partial\epsilon_1/\partial\Lambda)^{-1}$ and $\eta=\beta_1(\partial\epsilon_1/\partial\Lambda)^{-1}$. On substituting the solution α_1 of (30) into the remaining equations in the system, we find the first order components γ_2, γ_3,... of the amplitude. Note, that the nondegeneracy of the zero eigenvalue is important at this stage and guarantees the smallness of γ_2, γ_3,... . Finally, we go to second order in our perturbation scheme

$$\mathbf{D}\cdot\mathbf{A}_2=\mathbf{C}+\mathbf{Q}^{-1}\cdot\dot{\mathbf{A}}_1$$

with $\mathbf{C}$ representing all algebraic second-order corrections including products of zero- and first-order amplitudes. Multiplication of the last equation by $\mathbf{e}_1^T$ from the left yields the slow equation for the last remaining first-order component γ_1 in the problem

$$\mathbf{e}_1^T\cdot[\mathbf{C}+\mathbf{Q}^{-1}\cdot\dot{\mathbf{A}}_1]=0. \tag{31}$$

This completes our perturbation analysis. Its main results are (a) the quasilinear evolution equation (30) describing zero order amplitude α_1 of a driven, m-fold symmetric vortex pack, and (b) the proof of the smallness of all first-order corrections γ_i to the amplitude, justifying the perturbation expansion.

IV. SYNCHRONIZED DYNAMICS OF A VORTEX PACK

Here, we analyze adiabatic passage through resonance $m\Omega(t)-\Lambda\approx 0$ with the nondegenerate eigenfrequency Λ, associated with the zero eigenvalue ϵ_1 (see above) in our system, as described by the weakly nonlinear equation (30). The spectrum of eigenfrequencies Λ depends on the choice of initial axisymmetric vorticity distribution. Consider distribution (3) as an example. We discretize this distribution and view it as a superposition of N centered uniform vortices of radii $a_n=n/N$ and vorticities ω_n as described in Sec. II. Figure 8 (solid lines) shows the spectrum of Λ (for $N=13$) in $m=3$ case versus vorticity distribution parameter κ. We see that the spectrum consists of a closely packed group of 12 eigenfrequencies and an additional, well separated, single $\Lambda=\Lambda_0$. The averaged separation between the eigenfrequencies in the closely packed group in our example decreases with N (roughly as $1/N$) and, therefore, we associate this group with the continuum spectrum in the limit $N\to\infty$. The separated eigenfrequency Λ_0 represents the discrete mode in this limit. The eigenspectrum for other values of m are similar with one exception for $m=1$. In this case $\Lambda_0=0$ for all κ, i.e., this separated mode is stationary, it simply represents a displaced original axisymmetric vortex.

It is important, at this stage, to discuss the distribution of fluid rotation velocities in the unperturbed vortex. For given

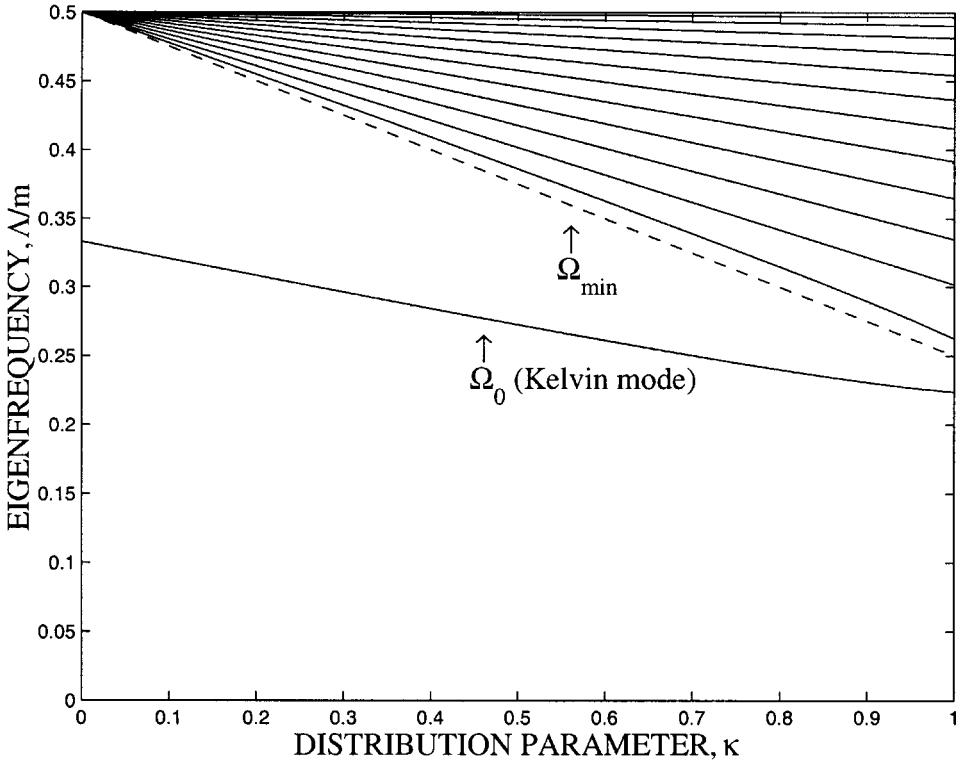

FIG. 8. Eigenfrequencies (solid lines) of discretized ($N=13$) vorticity distribution for $m=3$ case versus distribution parameter κ. The dashed line shows the frequency $\Omega_{\min}$ of the fluid rotation at the boundary of the unperturbed axisymmetric vortex (this is the lowest rotation frequency of the fluid inside the vortex). The system has a single, well separated Kelvin mode having frequency Ω_0 below $\Omega_{\min}$.

radius r, the unperturbed fluid rotation frequency is $\bar{\Omega}=r^{-2}\int_0^r \omega(r')r'\,dr'$. Then, inside the vortex ($0<r<1$), vorticity distribution (3) yields $\bar{\Omega}=\frac{1}{2}[1-(\kappa r^2/2)]$. These rotation frequencies are distributed in the interval $[\Omega_{\min},0.5]$, where the lowest frequency $\Omega_{\min}=\frac{1}{2}[1-(\kappa/2)]$ corresponds to the boundary of the vortex ($r=1$). We show $\Omega_{\min}$ by a dashed line in Fig. 8. We observe in the figure that all eigenfrequencies Λ/m in the closely packed part of spectrum are in the interval $[\Omega_{\min},0.5]$ and, therefore, satisfy resonance condition $\Lambda/m=\bar{\Omega}(r_{\rm res})$ at some point $r_{\rm res}$ *inside* the unperturbed vortex. As a consequence, these modes are Landau damped in the continuum limit.[12] The well separated mode frequency Ω_0, in contrast, is outside this interval, so this mode comprises an *undamped*, Kelvin mode [which still may be subject to other types of instabilities (see the next section)]. The existence of the Kelvin mode is due to the compactness and steep edges of our vortex. Other cases, characteristic to vorticity distributions with extended edges and having only continuum spectra, were studied in Refs. 12 and 18. We shall limit our discussion below to passage through a single, well separated, undamped Kelvin mode, use vorticity distribution (3) as a representative example, and postpone the study of passage through a closely packed group of eigenfrequencies to future work.

The well separated mode in our problem has a unique spatial structure and we discuss this structure next. One finds, that all the components of the zero eigenvector $\mathbf{e}_1$ characterizing the mode have the same sign. By returning to the original dependent variable $\mathbf{Z}$ [in components $Z_n=\delta_n\exp(im\theta_n)$], we have $\mathbf{Z}=\mathbf{Q}^{-1}\cdot\mathbf{W}\exp[-im\int\Omega(t)dt]$ or, on using (29),

$$\mathbf{Z}\approx\alpha_1\mathbf{Q}^{-1}\cdot\mathbf{e}_1\exp\left[i\Theta-im\int\Omega(t)dt\right]. \tag{32}$$

Then, by introducing the absolute value and imaginary phase of α_1, i.e., writing $\alpha_1=a\exp(i\phi)$, we find $\delta_n\approx a d_n$, where $d_n=(\omega_n a_n^2)^{-1}e_{1n}$, while all inclinations θ_n are the same $m\theta_n=\Theta-m\int\Omega(t)dt+\phi\equiv-\Phi$. Furthermore, since all the components e_{1n} of $\mathbf{e}_1$ have the same sign, all δ_n are also single signed. In other words, all vortex patches comprising the discrete mode are *positioned similarly* in space at all times [as shown in Figs. 1(b)–1(d)], illustrating that the associated deformation is analogous to a rigidly rotating Kelvin mode.

Now, we proceed to studying the evolution of the amplitude α_1 characterizing the discrete mode. We separate the real and imaginary parts in Eq. (30), yielding

$$\dot{a}=-\eta\sin\Phi, \tag{33}$$

$$\dot{\Phi}=m\Omega(t)-\Lambda_0+pa^2-\eta a^{-1}\cos\Phi, \tag{34}$$

where the phase mismatch $\Phi=m\int\Omega(t)dt-\Theta-\phi$ was defined above. Next, we assume linear sweeping of the external rotation frequency $\Omega(t)=\Omega_0-\alpha t$, $\alpha>0$ ($\Omega_0=\Lambda_0/m$ is the linear resonant frequency used in our simulations in Sec. II), and rewrite Eqs. (33) and (34) in the form

$$\frac{d\Delta}{d\tau}=-\eta_0\sin\Phi, \tag{35}$$

$$\frac{d\Phi}{d\tau}=-\tau+\Delta^2-\eta_0\Delta^{-1}\cos\Phi, \tag{36}$$

where, the rescaled dimensionless time, amplitude and strain rate are $\tau=(m\alpha)^{1/2}t$, $\Delta=p^{1/2}(m\alpha)^{-1/4}a$, and $\eta_0=p^{1/2}(m\alpha)^{-3/4}\eta$, respectively. Remarkably, we have reduced the problem to a single parameter (η_0) system of evolution equations (35) and (36). Furthermore, we observe that the form of these equations is the same as those describing synchronization of a *single* driven vortex patch,[5,17] so we can apply all the conclusions of that theory to our multicontour system. For example, at certain conditions, the discrete mode starting from $\Delta=0$ at large negative τ, will adjust its internal state to remain phase locked with the external rotation at large positive τ, i.e., beyond the linear resonance and despite variation of the external rotation frequency. In other words, we asymptotically approach the solution $\Delta\approx\tau^{1/2}$ at positive τ. This means excitation of a growing amplitude, m-fold symmetric state (which later extends beyond the weakly nonlinear stage, until filaments develop in the vortex patch with largest a_n) as illustrated in examples in Sec. II. The condition for entering this phase locked solution is translated into a condition on the single parameter η_0 in the problem. One finds that there exists a critical value $\eta_{0\text{th}}$ such that the persisting phase locking in the system occurs for $\eta_0>\eta_{0\text{th}}$ only. By returning to our original parameters, we then obtain the threshold condition

$$\eta>\eta_{\text{th}}=\eta_{0\text{th}}(m\alpha)^{3/4}p^{-1/2}. \tag{37}$$

The theory yielding an estimate for $\eta_{0\text{th}}$ is simple,[17] and we present it below for completeness.

Let us assume a continuing phase locking $\Phi\approx 0$ in the system as it passes the linear resonance point and, consequently, replace $\cos\Phi$ in Eq. (36) by unity. Then, let us differentiate the resulting equation in time and substitute Eq. (35) for $d\Delta/d\tau$, yielding

$$d^2\Phi/d\tau^2=-1-\eta_0 S\sin\Phi, \tag{38}$$

where $S=2\Delta+\eta_0/\Delta^2$. Equation (38) describes a quasiparticle in tilted cosine quasipotential:

$$V_{\text{eff}}(\Phi)=\Phi-\eta_0 S\cos\Phi, \tag{39}$$

where parameter S is a function of time via varying Δ. The potential $V_{\text{eff}}(\Phi)$ possesses minima only if $\eta_0 S>1$. Otherwise, $V_{\text{eff}}(\Phi)$ increases monotonically. The existence of the potential minima is necessary for having trapped solutions, i.e., phase locking in our real problem, where Φ describes the phase mismatch between the external rotation and the quasi-Kelvin mode. On the other hand, S has a minimum $S_m=3\eta_0^{1/3}$ at $\Delta_m=\eta_0^{1/3}$. Substitution of S_m into $\eta_0 S>1$ yields the threshold condition $\eta_0>\eta_{0\text{th}}=3^{-3/4}=0.439$. By solving Eqs. (35) and (36) numerically, starting at large negative τ, one finds a slightly lower value $\eta_{0\text{th}}=0.411$, which we shall use in Eq. (37) in the following.

At this point we recall that the nonlinearity was added in our theory via heuristic arguments. The value of the nonlinearity parameter p in our multicontour pack case is still unknown. Nonetheless, since the threshold for capture into resonance is sensitive to parameters and form the nonlinearity, it can be used for both testing our choice of the form of nonlinearity and estimating p from simulations. This worked as follows. We calculated the threshold value η_{th} in a given case (for some κ, and α) by using CD simulations. Then Eq. (37), yielded p for this case. For instance, in $\kappa=0.6$ case, for all α (the scaling with α can be seen in the example in Fig. 5), we found $p=1.45$, and 4.75 for $m=2$, and 3, respectively. Finally, we used these values of p in several examples in comparing the whole evolution of the emerging coherent nonuniform V-states, as predicted by the reduced pair of phase-amplitude equations (35) and (36), with CD simulation results. We found excellent agreements between the two calculations in all cases considered (compare circles and full lines in Figs. 2 and 6).

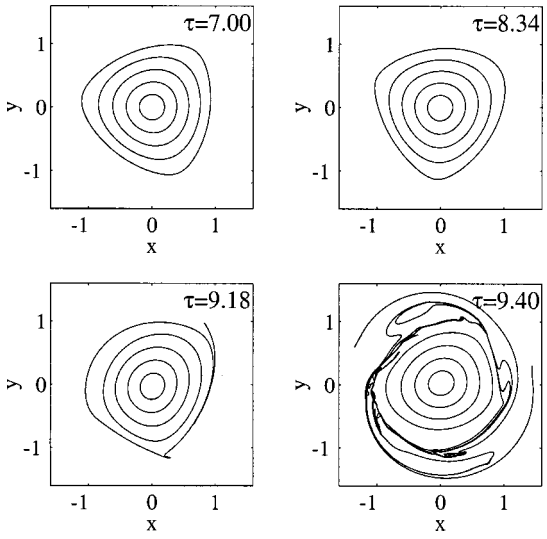

FIG. 9. The snapshots of unstable, $m=3$ vortex [case (b) in Fig. 4] at times $\tau=7.00$, 8.34, 9.18, and 9.40. The azimuthal symmetry of the vortex is destroyed as the result of the instability.

V. STABILITY OF MULTICONTOUR STATES

In this section, we discuss the problem of stability of nonuniform V-states. Numerical simulations showed that free (unstrained) $m=2$ states, excited by passage through resonance and synchronization were stable. In contrast, $m=3$ states developed instability (the difference between the two cases can be seen by comparing Figs. 2 and 4). The snapshots of the actual vortex developing the instability [for case (b) in Fig. 4] are shown in Fig. 9. The snapshots are taken at $\tau=7.00$, 8.34, 9.18, and 9.40 and illustrate how the instability destroys $m=3$ azimuthal symmetry, i.e., leads to appearance of other m components in the solution. Free $m=4$ multicontour V-states excited by passage through resonance [see Fig. 1(d)] were also unstable and decayed similarly to the $m=3$ case. Since the treatment of both cases is similar, we shall limit our discussion in this section to the decay of $m=3$ V-state only. In order to understand this instability we further analyzed our simulation results and presented this analysis in Figs. 10 and 11. Again, we considered a multicontour V-state excited by passage through $m=3$ resonance [case (c) in Fig. 4]. We focussed on the free vortex stage in Fig. 4, i.e., $\tau>\tau_1=1$, and expanded the numerically found radius $r_5(\varphi,t)$ of the outer ($n=5$) contour in Fourier series

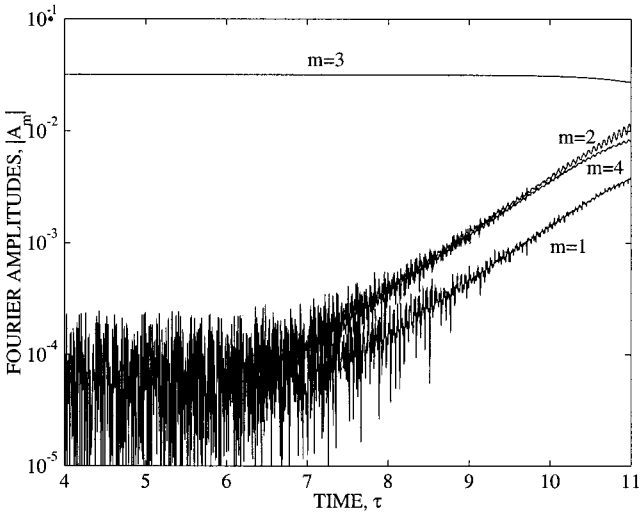

FIG. 10. The evolution of azimuthal $m=1$, 2, 3, and 4 components in the multicontour *V*-state excited by passage through $m=3$ resonance. $m=1$, 2, and 4 modes at early times grow exponentially from noise via resonant three-wave interactions driven by $m=3$ mode.

$$r_5(\varphi,t)=\sum_{-\infty}^{\infty} A_m(t)\exp(im\varphi).$$

The evolutions of the absolute values $|A_m|$ of the amplitudes of $m=1$, 2, 3, and 4 components in this series are shown in Fig. 10. One can see that initially, the free vortex has mostly the expected $m=3$ component, other m components appear as a numerical noise. However, at later times, $m=1$, 2, and 4 components grow exponentially. Also, all growth rates of these unstable modes are the same, until saturation stage, where the instability starts affecting the main $m=3$ component.

In order to obtain further information, we performed time-Fourier analysis of each of the m components in the series and calculated

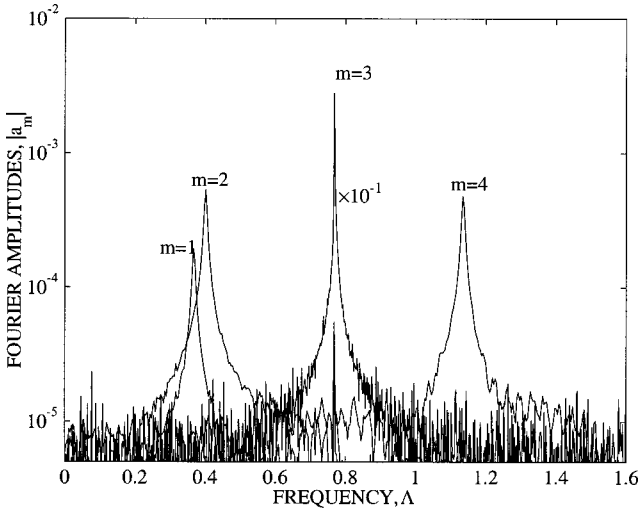

FIG. 11. The frequency spectrum of the multicontour *V*-state excited by passage through $m=3$ resonance. Peak frequencies Λ'_m of $m=1$, 2, 3, and 4 components satisfy three-wave resonant conditions $\Lambda'_3=\Lambda'_1+\Lambda'_2$ and $\Lambda'_3=\Lambda'_4-\Lambda'_1$.

$$a_m(\Lambda)=\int_{\tau_1}^{\tau_2} A_m(t)\exp(-i\Lambda t)dt,$$

$\tau_2=11$ being the end time point in Fig. 10. The resulting spectra $|a_m|$ are presented in Fig. 11. We see sharp peaks in the spectra and find that the frequencies Λ'_m of these peaks and, to great accuracy, satisfy the following three-wave resonant $\Delta'_{123}=\Lambda'_3-\Lambda'_1-\Lambda'_2=0$ and $\Delta'_{134}=\Lambda'_4-\Lambda'_3-\Lambda'_1=0$ ($|\Delta'_{123}|/\Lambda'_1$ and $|\Delta'_{123}|/\Lambda'_1$ are less than 10^{-4}). We also notice the characteristic Lorentzian form of these peaks. All these results clarify the situation. One expects this type of spectra if each of the unstable A_m components has the form

$$A_m(t)=A_{m0}\exp[(i\Lambda'_m+\lambda)t], \quad m=1,2,4, \tag{40}$$

where λ is real, positive and the same for all m. Then

$$|a_m(\Lambda)|\approx|A_m(\tau_2)|[(\Lambda-\Lambda'_m)^2+\lambda^2]^{-1/2}. \tag{41}$$

Similar, Lorentzian shapes for all exponentially growing modes can be seen in Fig. 11. The main ($m=3$) mode, which is only weakly damped in the initial stage of instability, has a much sharper peak in Fig. 11. The reason for the instability in our piecewise-constant vorticity evolution problem can be attributed to resonant three-wave interactions driven by a large, nearly constant amplitude $m=3$ mode. The process is analogous to the beat-wave resonance decay instability discussed in the past in application to continuous vorticity distributions.[19,20] Indeed, we find that the frequencies Λ'_m are slightly shifted eigenfrequencies in the *linear* spectrum of the corresponding modes (see Sec. IV). Furthermore, $\Lambda'_{2,3,4}$ are near eigenfrequencies Λ_{m0} of linear Kelvin modes of corresponding m, while Λ'_1 is near the lowest eigenfrequency $\Lambda_{1\,\min}$ in the closely packed part of the spectrum for $m=1$ (recall that the Kelvin mode frequency in $m=1$ case vanishes). These linear modes, in our case, satisfy *approximate* three-wave resonance conditions $\Delta_{123}=\Lambda_{30}-\Lambda_{1\,\min}-\Lambda_{20}=0.07\Lambda_{1\,\min}$ and $\Delta_{134}=\Lambda_{40}-\Lambda_{1\,\min}-\Lambda_{30}=0.035\Lambda_{1\,\min}$. Therefore, second-order interactions between the Kelvin modes in two triads of waves ($m=1,2,3$, and 1,3,4) introduce beat-frequency drive resonating with the $m=1$ mode (in the closely packed group of the spectrum). These resonant interactions do not affect nonlinear frequency shifts of the interacting modes, but may lead to instabilities, as seen in Figs. 4 and 9. Let us discuss this phenomenon in more detail.

In the preceding sections we focused on the main, single m mode, and neglected resonant interactions between modes having different m. Formally, one can include these effects in the problem by adding the usual three-wave resonant coupling terms in Eq. (30) for each mode. For example, resonant triads $m=1,2,3$, and 1,3,4 are described by

$$\dot{\alpha}_1=f_1\alpha_3\alpha_2^*e^{i\Delta_{123}t}+g_1\alpha_3^*\alpha_4e^{i\Delta_{134}t}, \tag{42}$$

$$\dot{\alpha}_2=f_2\alpha_3\alpha_1^*e^{i\Delta_{123}t}, \tag{43}$$

$$\dot{\alpha}_4=g_2^*\alpha_3\alpha_1e^{-i\Delta_{134}t}, \tag{44}$$

$$\dot{\alpha}_3=-ip|\alpha_3|^2\alpha_3, \tag{45}$$

where α_m denote complex amplitudes in Eq. (30) for corresponding m, the external strain is turned off, $f_{1,2}$ and $g_{1,2}$ are

constant mode coupling coefficients, and Δ_{123}, Δ_{134} are linear frequency detunings, as defined above. In writing Eqs. (42)–(45), we neglected nonlinear frequency shifts for small amplitude modes $m=1,2,4$ (these modes grow from noise), kept the third-order nonlinear term in the equation for the main mode $m=3$ only, but neglected, to lowest order, the effect of other modes on the main mode.

Now, we analyze solutions of Eqs. (42)–(45). First, we observe that Eq. (45) yields constant amplitude solution $\alpha_3 = \alpha_{30}\exp(i\nu_3 t)$, where $\nu_3 = -p|\alpha_{30}|^2$ represents the nonlinear frequency shift. Next, we seek solutions for the remaining amplitudes in the form [see Eq. (40)] $\alpha_m = \alpha_{m0}e^{\Gamma_m t}$ for $m=1$, 2, and 4, where α_{m0} and Γ_m are constants. We also assume that $\lambda = \mathrm{Re}\,\Gamma_m$ is common to all these modes, but $\nu_m = \mathrm{Im}\,\Gamma_m$ are generally different. Substitution of these solutions into our system yields

$$\Gamma_1\alpha_{10} = f_1\alpha_{30}\alpha_{20}^* e^{i\Delta'_{123}t} + g_1\alpha_{30}^*\alpha_{40}e^{i\Delta'_{134}t}, \tag{46}$$

$$\Gamma_2\alpha_{20} = f_2\alpha_{30}\alpha_{10}^* e^{i\Delta'_{123}t}, \tag{47}$$

$$\Gamma_4\alpha_{40} = g_2^*\alpha_{30}\alpha_{10}e^{-i\Delta'_{134}t}, \tag{48}$$

where $\Delta'_{123} = \Delta_{123} + \nu_3 - \nu_1 - \nu_2$ and $\Delta'_{134} = \Delta_{134} - \nu_3 - \nu_1 + \nu_4$. Then, the assumed constancy of α_{m0} yields

$$\Delta'_{123} = \Delta'_{134} = 0, \tag{49}$$

i.e., $\Gamma_2 = \Gamma_1^* + i\gamma_2$, $\Gamma_4 = \Gamma_1 + i\gamma_4$, where $\gamma_2 = \Delta_{123} - p|\alpha_{30}|^2$ and $\gamma_4 = -\Delta_{134} - p|\alpha_{30}|^2$. Then, the use of Eqs. (47), (48) in (46) leads to the equation for Γ_1:

$$\Gamma_1 = \left(\frac{f_1 f_2^*}{\Gamma_1 - i\gamma_2} + \frac{g_1 g_2^*}{\Gamma_1 + i\gamma_4}\right)|\alpha_{30}|^2. \tag{50}$$

Note that real frequencies of the *interacting* ($m=1$, 2, 3, and 4) modes are $\Lambda'_{mi} = \Lambda_{m0} + \nu_m$ and, therefore, Eqs. (49) express exact resonance conditions $\Lambda'_3 - \Lambda'_1 - \Lambda'_2 = 0$ and $\Lambda'_4 - \Lambda'_1 - \Lambda'_3 = 0$, as was seen in our simulations.

The simplest situation described by Eq. (50) corresponds to large Γ_1, when one can neglect $\gamma_{2,4}$ in this equation. Then

$$\Gamma_1 = \pm(f_1 f_2^* + g_1 g_2^*)^{1/2}|\alpha_{30}| \equiv \pm\Gamma_{10}, \tag{51}$$

i.e., unstable, exponentially growing solution is obtained if $\mathrm{Arg}(f_1 f_2^* + g_1 g_2^*) \neq \pi$. In this case, the growth rate, $\lambda = |\mathrm{Re}\,\Gamma_1|$, of all unstable modes is the same (as found in our simulations) and scales as $\lambda \sim |\alpha_{30}|$. In contrast, as $|\alpha_{30}| \to 0$, Eq. (50) becomes

$$\Gamma_1 = \left(\frac{f_1 f_2^*}{\Gamma_1 - i\Delta_{123}} + \frac{g_1 g_2^*}{\Gamma_1 - i\Delta_{134}}\right)|\alpha_{30}|^2, \tag{52}$$

yielding three approximate solutions: $\Gamma_1^{(1)} \approx i(f_1 f_2^*/\Delta_{123} + g_1 g_2^*/\Delta_{134})|\alpha_{30}|^2$, $\Gamma_1^{(2)} \approx i\Delta_{123} - i(f_1 f_2^*/\Delta_{123})|\alpha_{30}|^2$, and $\Gamma_1^{(2)} \approx i\Delta_{134} - i(g_1 g_2^*/\Delta_{134})|\alpha_{30}|^2$. Thus, the growth rate scales as $\lambda \sim |\alpha_{30}|^2$ for small $|\alpha_{30}|$. We have tested these predictions numerically. Figure 12 shows the rescaled growth rate, $\bar{\lambda} = \lambda t_r$ [t_r being the period of rotation of the main excited ($m=3$) mode] as found in simulations versus amplitude $|\alpha_{30}|$. The circles in the figure are the results from our simulations, while the two dashed lines represent limiting $\lambda \sim |\alpha_{30}|$ and $\lambda \sim |\alpha_{30}|^2$ scalings.

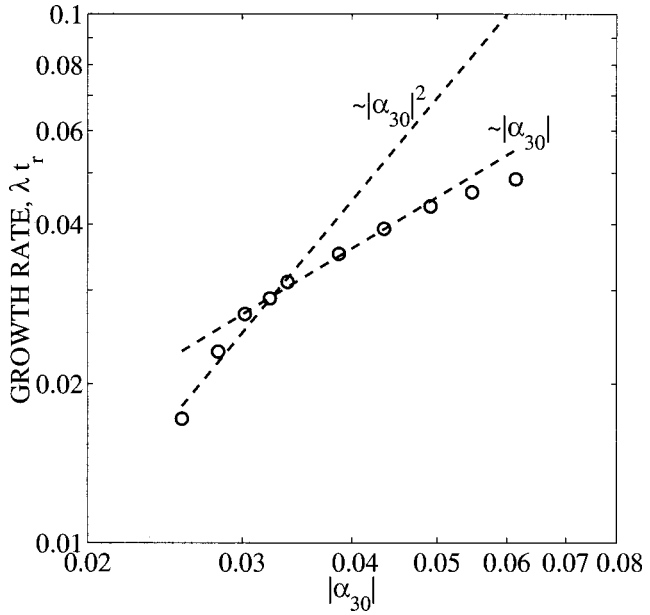

FIG. 12. The numerical (circles), rescaled growth rate, $\bar{\lambda} = \lambda t_r$ (t_r being vortex rotation frequency) of $m=1$, 2, and 4 modes, emerging in the decay of nonuniform $m=3$ V-state versus amplitude $|\alpha_{30}|$ of this state. The parameters are as in Fig. 4. The dashed lines represent limiting $\bar{\lambda} \sim |\alpha_{30}|$ and $\bar{\lambda} \sim |\alpha_{30}|^2$ scalings.

It is interesting to compare our results to those in experiments,[20] studying decay of nonaxisymmetric states of different m in non-neutral plasmas. The decay was explained in terms of the beat-wave resonance,[19] the growth rate scaled as $\lambda \sim |\alpha_{m0}|^2$, but, typically, λ was smaller than in Fig. 12 at comparable α_{m0}. The experimental conditions in Ref. 20 differed in several aspects from those assumed in our theory. For example, the plasma density distribution (the analog of vorticity distribution in fluid applications) was different and the experiments were done with a grounded wall (the $m=1$ Kelvin mode in Ref. 20 was due to induced image charges). Nevertheless, the decrease in the observed growth rates may be also explained by the presence of a substantial damping in the experiments. One can model such additional damping in our theory. Indeed, if one adds the linear damping term $-\chi\dot{\alpha}_1$ ($\chi > 0$ being the damping rate) in the RHS of Eq. (42), then Eq. (51) is replaced by

$$\Gamma_1(\Gamma_1 + \chi) = (f_1 f_2^* + g_1 g_2^*)|\alpha_{30}|^2 \equiv \Gamma_{10}^2, \tag{53}$$

yielding $\Gamma_1 = -\chi/2 \pm [(\chi/2)^2 + \Gamma_{10}^2]^{1/2}$. Therefore, when χ is sufficiently large ($|\Gamma_{10}|/\chi \ll 1$), one of the solutions

$$\Gamma_1 \approx \chi^{-1}\Gamma_{10}^2 = \chi^{-1}(f_1 f_2^* + g_1 g_2^*)|\alpha_{30}|^2 \tag{54}$$

yields instability if $\mathrm{Re}(f_1 f_2^* + g_1 g_2^*) > 0$. In this case λ is smaller by factor Γ_{10}/χ^{-1}, as compared with no damping case, and the growth rate scales as $\lambda \sim |\alpha_{30}|^2$.

The aforementioned analysis of three-wave resonant decay of $m=3$ multicontour V-states also suggests an approach to stabilization of this instability. The idea is to subject the unstable vortex structure to additional external strain, correlated with one of the unstable modes involved in the three-wave decay process. The goal is to create artificial damping of this parasitic mode and, thus, slow down or pre-

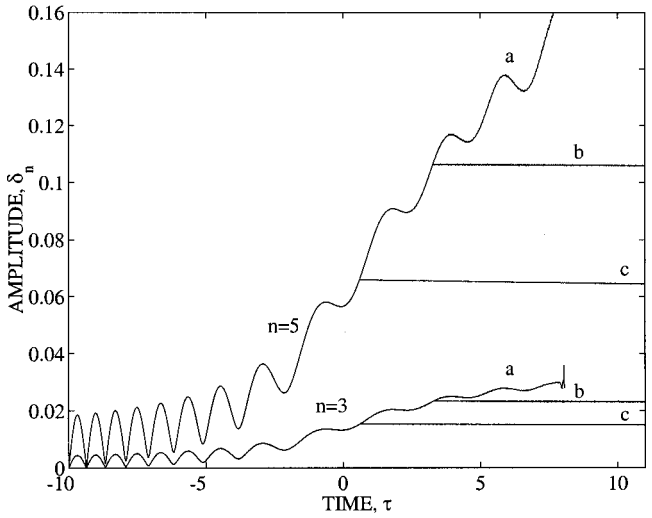

FIG. 13. Stabilization of nonuniform $m=3$ *V*-state by negative feedback method with damping of the $m=2$ mode (compare to unstable case shown in Fig. 4). The figure shows evolution of deformation amplitudes of $n=5$ and $n=3$ contours of stabilized $m=3$ *V*-state. Remaining contours evolve similarly. Curves (a) continuing linear sweep of the external rotation frequency; (b) the straining flow and variation of external rotation frequency are switched off beyond $\tau=3.3$; (c) the strain and variation of external rotation are switched off beyond $\tau=0.5$. The $m=3$ multicontour *V*-states remain stable, as long as the negative feedback drive is present.

vent exponential growth. A similar approach was used to either damp or excite diocotron modes in a number of experiments with pure electron plasmas.[21,22] We shall refer to the method as the *negative feedback stabilization* in the following. It works as follows. Suppose, one can measure the growing parasitic $m=2$ component of the flow in the vortex created by passage through resonance with the $m=3$ mode (in the pure electron plasma one simply measures the appropriate component of the electric potential on an external pickup electrode). Then, if one applies an additional $m=2$ external strain when resonantly driving the main $m=3$ mode, and (a) the additional strain amplitude is proportional to that of the measured $m=2$ signal and (b) its phase is properly shifted with respect to that of the measured signal, one introduces effective *exponential* damping in the system. If this dissipation is sufficiently strong, the three-wave decay can be efficiently prevented. We have performed CD simulations illustrating this idea and present the results of these calculations in Fig. 13. This figure is equivalent to Fig. 4, where we have seen the instability of the free vortex, but now we apply the negative feedback. The choice of our feedback strain was as in Eq. (2) used to drive the main ($m=3$) mode, but now we used $m=2$ and $\epsilon(t)=2|A_2|\sin[\arg(A_2)]$, where $A_2(t)$ was the time dependent component in the series $r_5(\varphi,t)=\Sigma_{-\infty}^{\infty}A_m(t)\exp(im\varphi)$ for the outer contour in the vortex pack. We found (see Fig. 13) that the resulting $m=3$ multicontour state was stable, as long as the negative feedback was present in the calculations.

The implementation of the negative feedback stabilization described above seems to be difficult in fluid experiments. Nevertheless, the negative feedback in analogous, non-neutral plasma experiments is a rather simple electronic routine, requiring detection of the electric potential induced by the desired mode on an external electrode, appropriate phase shifting and amplification of the detected signal and its application back to the plasma. This completes our discussion of stability of nonuniform *V*-states excited via synchronization approach.

VI. CONCLUSIONS

(i) We have studied excitation and control of nonuniform 2D *V*-states in free and bounded space by subjecting initially axisymmetric vorticity distribution with a sharp edge to a weak external strain and rotation with slowly varying rotation frequency. The desired nonuniform *V*-states emerged as the result of passage through resonance with the isolated eigenmode of the original vorticity distribution.

(ii) We developed our theory for a piecewise constant, initially axisymmetric vorticity distribution representing radially discretized continuous distribution with a sharp edge. This discretization corresponded to a superposition of a number of uniform vortex patches. We investigated driven dynamics of this vortex pack both numerically (via multicontour dynamics simulations) and theoretically within a weakly nonlinear reduced formalism. The formalism yielded a pair of phase-amplitude equations describing the driven system and having the form similar to that studied previously for driven uniform *V*-states, easing the understanding of the nonuniform case.

(iii) It was shown that the driven multicontour system enters a stage, where it is phase locked with slowly varying external rotation, provided the external strain rate is above a threshold, which scales as $\alpha^{3/4}$, where α is the sweep rate of the external rotation frequency. The sensitivity of the threshold to changes in parameters allowed to evaluate nonlinear frequency shift parameter in our problem, by comparing simulation results for the threshold with the theoretical scaling.

(iv) Above the threshold, the phase locking in the system meant a complete control of the *V*-state by shaping the time dependence of the external rotation appropriately. Thus, the resulting vortex could be viewed as a quasiparticle having complex, but robust internal structure, which can be conveniently manipulated by external perturbations.

(v) A similar approach based on passage through resonance and synchronization was used for excitation and control of more complex nonuniform vortex structures in bounded space regions. We have presented numerical examples of such nontrivial solutions emerging by passage through azimuthal $m=1$, 2, and 3 resonances.

(vi) Finally, we analyzed stability of nonuniform *V*-states excited by synchronization approach after the external strain and rotation were switched off. The $m=2$ state was stable, while $m=3$ and 4 states developed instability at later times. We have analyzed this effect and have shown that the instability is due to the resonant three-wave decay process involving other *m* modes excited from noise. We also suggested using the negative feedback approach to stabilize the instability and demonstrated this approach in simulations.

ACKNOWLEDGMENTS

We acknowledge the support by US-Israel Binational Science Foundation (Grant No. 1998474), by INTAS (Grant No. 99-1068), and RFBR (Grant No. 00-02-17179).

[1]G. S. Deem and N. J. Zabusky, ''Vortex waves: Stationary *V* states, interactions, recurrence, and breaking,'' Phys. Rev. Lett. **40**, 859 (1978).
[2]H. Lamb, *Hydrodynamics*, 6th ed. (Cambridge University Press, Cambridge, 1932), p. 232.
[3]C. H. Su, ''Motion of fluid with constant vorticity in a singly-connected region,'' Phys. Fluids **22**, 2032 (1979).
[4]P. G. Saffman, *Vortex Dynamics* (Cambridge University Press, Cambridge, 1992), Sec. 9.4.
[5]L. Friedland and A. G. Shagalov, ''Resonant formation and control of 2D symmetric vortex waves,'' Phys. Rev. Lett. **85**, 2941 (2000).
[6]L. Friedland, ''Migration timescale thresholds for resonant capture in the plutino problem,'' Astrophys. J. Lett. **547**, L75 (2001).
[7]J. Fajans, E. Gilson, and L. Friedland, ''Autoresonant (non-stationary) excitation of the diocotron mode in non-neutral plasmas,'' Phys. Rev. Lett. **82**, 4444 (1999).
[8]L. Friedland and A. G. Shagalov, ''Excitation of solitons by adiabatic multi-resonant forcing,'' Phys. Rev. Lett. **81**, 4357 (1998).
[9]For example, M. V. Melander, J. C. McWilliams, and N. J. Zabusky, ''Axisymmetrization and vorticity-gradient intensification of an isolated two-dimensional vortex through filamentation,'' J. Fluid Mech. **178**, 137 (1987).
[10]For example, D. G. Dritschel and B. Legras, ''The elliptical model of two-dimensional vortex dynamics. Part II: disturbance equations,'' Phys. Fluids A **3**, 855 (1991).
[11]D. G. Dritschel, ''On the persistence of non-axisymmetric vortices in inviscid two-dimensional flows,'' J. Fluid Mech. **371**, 141 (1998).
[12]D. A. Schecter, D. H. E. Dubin, A. C. Class, C. F. Driscoll, I. M. Lansky, and T. M. O'Neil, ''Inviscid damping of asymmetries on a two-dimensional vortex,'' Phys. Fluids **12**, 2397 (2000).
[13]N. J. Zabusky, M. H. Hughes, and K. V. Roberts, ''Contour dynamics for the Euler equations in two dimensions,'' J. Comput. Phys. **30**, 96 (1979).
[14]D. G. Dritschel, ''Contour dynamics and contour surgery: numerical algorithms for extended, high-resolution modelling of vortex dynamics in two-dimensional, inviscid, incompressible flows,'' Comput. Phys. Rep. **10**, 77 (1989).
[15]H. Lamb, *Hydrodynamics*, 6th ed. (Cambridge University Press, Cambridge, 1932), p. 231.
[16]P. G. Saffman, *Vortex Dynamics* (Cambridge University Press, Cambridge, 1992), Sec. 3.10.
[17]L. Friedland, ''Control of Kirchhoff vortices by a resonant strain,'' Phys. Rev. E **59**, 4106 (1999).
[18]N. J. Balmforth, S. G. L. Smith, and W. R. Young, ''Disturbing vortices,'' J. Fluid Mech. **426**, 95 (2001).
[19]J. D. Crawford and T. M. O'Neil, ''Nonlinear collective processes and the confinement of a pure-electron plasma,'' Phys. Fluids **30**, 2076 (1987).
[20]T. B. Mitchell and C. F. Driscoll, ''Symmetrization of 2D vortices by beat-wave damping,'' Phys. Rev. Lett. **73**, 2196 (1994).
[21]J. H. Malmberg, C. F. Driscoll, B. Beck, D. L. Egglston, J. Fajans, K. Fine, X. P. Huang, and A. W. Hyatt, in *Non-neutral Plasma Physics*, edited by C. Roberson and C. Driscoll (AIP, New York, 1988), Vol. 175, p. 28.
[22]J. Fajans, E. Gilson, and L. Friedland, ''The effect of damping on autoresonant (non-stationary) excitation,'' Phys. Plasmas **8**, 423 (2001).